Hydrol. Earth Syst. Sci., 17, 3779–3794, 2013
www.hydrol-earth-syst-sci.net/17/3779/2013/
doi:10.5194/hess-17-3779-2013


Hydrology and Earth System Sciences
Open Access

# Satellite-based analysis of recent trends in the ecohydrology of a semi-arid region

**M. Gokmen[1], Z. Vekerdy[1], W. Verhoef[1], and O. Batelaan[2,3]**

[1]Department of Water Resources, Faculty of Geo-Information Science and Earth Observation (ITC), University of Twente, Enschede, the Netherlands
[2]Department of Hydrology and Hydraulic Engineering, Vrije Universiteit Brussel, Brussel, Belgium
[3]School of the Environment, Flinders University, Adelaide, Australia

*Correspondence to:* M. Gokmen (mustaf.gokmen@gmail.com)

Received: 25 April 2013 – Published in Hydrol. Earth Syst. Sci. Discuss.: 16 May 2013
Revised: 16 August 2013 – Accepted: 28 August 2013 – Published: 7 October 2013

**Abstract.** We present a regional framework for an integrated and spatiotemporally distributed assessment of human-induced trends in the hydrology and the associated ecological health of a semi-arid basin where both human activities (i.e. agriculture) and natural ecosystems are highly groundwater dependent. To achieve this, we analysed the recent trends (from year 2000 to 2010) in precipitation, evapotranspiration (actual and potential) and vegetation greenness (i.e. NDVI) using a combination of satellite and ground-based observations. The trend assessment was applied for the semi-arid Konya Basin (Turkey), one of the largest endorheic basins in the world.

The results revealed a consistent increasing trend of both yearly evapotranspiration (totally 63 MCM $yr^{-1}$ from croplands) and mean NDVI (about 0.004 NDVI $yr^{-1}$ in irrigated croplands), especially concentrating in the plain part of the basin, while no significant trends were observed for the precipitation and potential evapotranspiration variables. On the contrary, a consistent decreasing trend of both yearly evapotranspiration (totally $-2.1$ MCM $yr^{-1}$) and mean NDVI ($-0.001$ NDVI $yr^{-1}$) was observed in the wetlands, which also cannot be explained by trends in precipitation and potential evapotranspiration. The emerging picture suggest that the greening trend of the vegetation and increasing of evapotranspiration in the plain are related to land cover changes (i.e. conversion into irrigated croplands) and to the intensification of the supplementary irrigation for agriculture, which in turn caused drying out of some wetlands and the natural vegetation which mostly depend on the groundwater, the main source of irrigation water as well.

Our study presented an example of the utility of spatially and temporally continuous RS data in assessing the regional trends in hydrological and ecological variables and their interactions in a spatially distributed manner in a semi-arid region, which can also be adapted to other regions. Such spatiotemporally distributed analysis at the basin level is particularly important considering that most of the water management interventions also take place at this scale.

## 1 Introduction

In recent years, the response of water cycle components and vegetation to the changing climate and anthropogenic effects has been discussed and studied widely at global and regional scales (e.g. Liu et al., 2013; Douville et al., 2012; Fensholt et al., 2012; Liu and Yang, 2010; Jung et al., 2010; Zhang et al., 2009; Milliman et al., 2008). Satellite observations have been increasingly used in such studies, exploiting their potential of providing spatially continuous and temporally recurrent estimates over regional to global scales (Alsdorf and Lettenmaier, 2003).

New et al. (2001) used gauge and satellite/merged precipitation data to analyse trends over global land areas in the twentieth century and found a century-long trend of 9 mm, which was considered quite small compared with multi-decadal (and also interannual) variability of precipitation. Also, Zhang X. B. et al. (2007) used monthly precipitation observations over global land areas to analyse precipitation trends in two twentieth century periods (1925–1999 and

1950–1999), and showed that anthropogenic forcing has had a detectable influence on observed changes in average precipitation within latitudinal bands, and that these changes cannot be explained by internal climate variability or natural forcing. Apart from global-scale studies, others (e.g. Du et al., 2011; Fensholt and Rasmussen, 2011; Lebel and Ali, 2009; Hatzianastassiou et al., 2008; Zhang et al., 2005) assessed the regional/continental precipitation trends and showed their influences on stream flow, water level, soil moisture and vegetation changes.

Jung et al. (2010) assessed the trends in the global land evapotranspiration (ET) and its spatial distribution over the past 27 yr. They compared the ET trends and their distribution with the trends in global potential evapotranspiration (PET) and soil moisture distributions, and showed increasing soil-moisture limitations on evapotranspiration largely explain the recent decline of the global land-evapotranspiration trend. On the other hand, Zhang et al. (2012) assessed the decadal trends in global evaporation using satellite and gridded meteorological data, and found that evaporation estimated from water balances of 110 "wet" and 87 "dry" catchments do not match with the estimates from three alternative ET models. On these lines, Teuling et al. (2009) put forward a regional perspective on the trends in evaporation, identifying that the trends in evapotranspiration (and hence runoff) can only be understood regionally (and temporally) by considering regional (and temporal) variations in the main drivers of evapotranspiration, because the controlling mechanisms of ET (i.e. energy demand and moisture supply) vary from region to region. Accordingly, several studies (Morrow et al., 2011; Zhang et al., 2001, 2009; Zhang Y. Q. et al., 2007; Ryu et al., 2008) conducted regional or catchment scale analysis of trends in ET based on satellite observations, meteorological data, water balance and energy balance approaches.

With respect to vegetation trends, satellite-based vegetation indexes such as normalized difference vegetation index (NDVI) are widely used to examine the dynamics of vegetation health, density, land cover and phenological changes. However, it remains a challenge to produce a long-term, consistent, vegetation index time series across the sequence of multiple sensor systems, not only due to their different spectral responses, spatial resolutions, swath width and orbiting geometry but also sensor degradations and drift in satellite overpass times. Therefore, several studies (Fensholt and Proud, 2012; Fensholt and Rasmussen, 2011; Beck et al., 2011; Alcaraz-Segura et al., 2010, among others) focused on intercomparisons between different sensor data sets. Other studies (e.g. Fensholt et al., 2012; Fensholt and Proud, 2012; Fensholt and Rasmussen, 2011; Heumann et al., 2007; Julien et al., 2006; Evans and Geerken, 2004) used NDVI time series to assess the trends and the responses of vegetation greenness to the changes in the climatic (e.g. rainfall and air temperature) or anthropogenic drivers.

Apart from analysing the trends, some studies (Douville et al., 2012; Milliman et al., 2008; Zhang X. B. et al., 2007; Evans and Geerken, 2004; Sharma et al., 2000) particularly focused on attributing these trends either to the changes in climatic variables (e.g. incoming radiation and temperature changes) or to anthropogenic effects (e.g. changes in land use or land cover). While some others also looked at the associated changes in the water budget and resources (Wada et al., 2012; Famiglietti et al., 2011; Morrow et al., 2011; Rodell et al., 2007, 2009; Tiwari et al., 2009; Zhang et al., 2009; Yang et al., 2007; Konikow and Kendy, 2005) and showed increase of nonrenewable groundwater depletion and increase/decrease of river discharges in different regions.

Detection of trends and their significance generally requires consistent and long-term records of variables. However, some human-induced trends such as land-use changes are likely to have an important role regionally (Jung et al., 2010) and, if severe, their impacts can be detected in relatively short periods. For example, assessing the satellite-based estimates of groundwater depletion in India during six years, Rodell et al. (2009) stated that despite the relatively short period of evaluation, other evidences supported their conclusion that severe groundwater depletion is occurring as a result of human consumption rather than natural variability. As revealed by many other studies (Famiglietti et al., 2011; Scanlon et al., 2010; McGuire, 2009; Rodell et al., 2009; Tiwari et al., 2009; Karami and Hayati, 2005; Konikow and Kendy, 2005), persistent groundwater depletion have been occurring in different regions, leading to falling groundwater levels (Gleeson et al., 2010). The results of a global scale study by Wada et al. (2012) show that nonrenewable groundwater abstraction (to sustain irrigation) globally contributes nearly 20 % to the gross irrigation (for the year 2000) and has more than tripled since 1960. Groundwater is not only essential to global food security providing an irrigation buffer against climate extremes but also affects terrestrial ecosystems by sustaining river base-flow and root-zone soil water in the absence of rain (Fan et al., 2013). Therefore, the value of groundwater is expected to increase in coming decades as temporal variability in precipitation, soil moisture and surface water are projected to increase under more frequent and intense climate extremes associated with climate change (Taylor et al., 2013), and also along with the rising population and their food demands, particularly in emerging countries such as India, Pakistan, China, Iran, Mexico and Turkey, among others. The semi-arid Konya Basin in central Anatolia (Turkey), which is one of the biggest endorheic basins in the world, is a characteristic example of groundwater resources under strong anthropogenic pressure. Over the last few decades, the basin experienced huge non-renewable groundwater abstraction for irrigation, which caused approximately 1 m $yr^{-1}$ head decline (Bayari et al., 2009).

In this study, we analyse the recent trends (from year 2000 to 2010) in precipitation, evapotranspiration (actual and potential) and vegetation greenness (i.e. NDVI) using satellite-based observations. On this basis, we assess the distribution

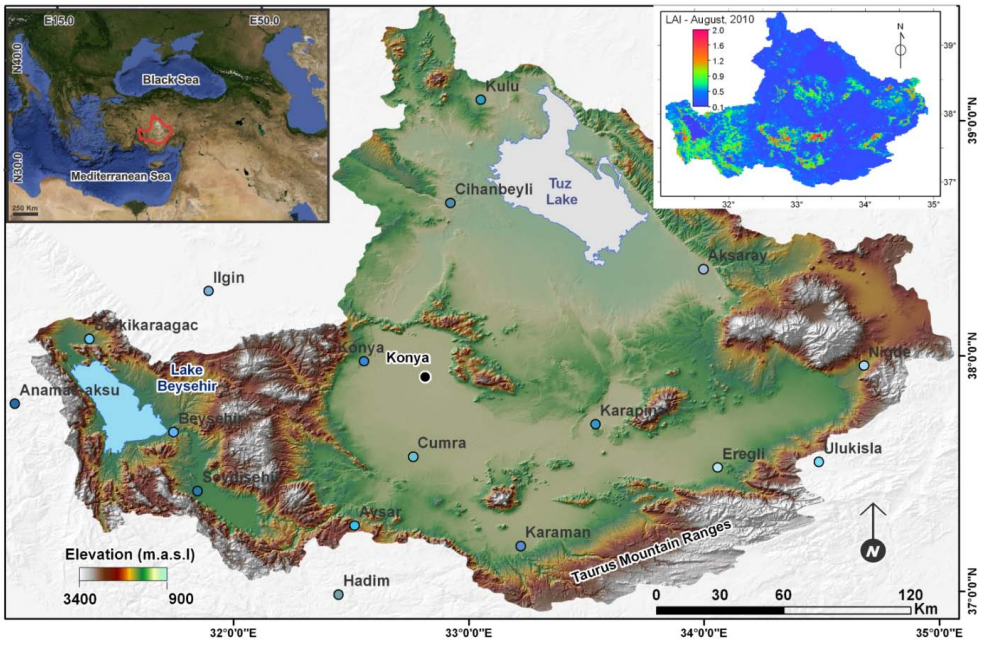


**Fig. 1.** The geographic location (top left), vegetation distribution (leaf area index map, top right), and SRTM-based elevation map with the locations of the meteorological stations (main panel) of the study area (adapted from Gokmen et al., 2012).

of the human-induced changes in the hydrology and the associated ecological health of the semi-arid Konya Basin where both human activities (agriculture) and natural ecosystems are highly groundwater dependent. More specifically, this study aims at

1. Providing a framework for a RS-based and integrated assessment of ecohydrological trends and their causes at regional scale.

2. Detecting trends and their significance in consistently established time series of actual and potential evapotranspiration, precipitation, vegetation greenness (i.e. NDVI) in a spatially distributed manner.

3. Inter-comparison of the observed trends and analysing the correlations in order to identify consistencies and to attribute them to the climate and/or human-induced changes.

4. Analysing inter-relations between the trends in the hydrological variables and the ecological health in the region.

## 2 Materials and methods

### 2.1 The study area

The Konya Basin is located in central Anatolia, Turkey, between 36.8° N, 31.0° E and 39.5° N, 35.1° E. The basin covers a surface area about 54 000 km$^2$, with elevations ranging from 900 to 3500 m above sea level (Fig. 1). There are extensive plains in the central and downstream areas, making the Konya Basin one of the most important agricultural regions of Turkey. Parts of these plains are occupied by two large lakes: the hyper-saline Tuz Lake in the downstream part and the freshwater Lake Beysehir in the upstream part. Numerous smaller fresh/brackish water bodies and wetlands were present in the mid- and downstream areas, and some of which have dried out in the last decades.

The region has a typical arid to semi-arid climate with a long-term average yearly precipitation of 380 mm (unpublished data from State Hydraulic Works, DSI), spatially ranging from 250 mm in the plain parts up to more than 1000 mm in the mountainous areas (Gokmen et al., 2013). The summers are hot and dry (with a maximum temperature reaching $\sim 40\,^{\circ}$C) whereas winters are cold and wet (the minimum temperature may go down to $\sim -20\,^{\circ}$C). While the southwestern upstream part shows a warmer and wetter Mediterranean character, the rest of the basin has a drier, continental climate, isolated from the moderating effect of the Mediterranean Sea by the Taurus mountains in the south.

The land cover in the low-lying areas of the basin shows a strong contrast between intensively irrigated agricultural lands and the sparsely vegetated steppe areas covering the mid- and downstream plains (Fig. 2a), where natural vegetation is dominated by Artemisia grasses (Fontugne et al., 1999). The adaptation methods of the natural vegetation to drought stress differ between the downstream area where the groundwater is shallow and soils are saline, and the rest of the region, where the groundwater table is located between 35 to

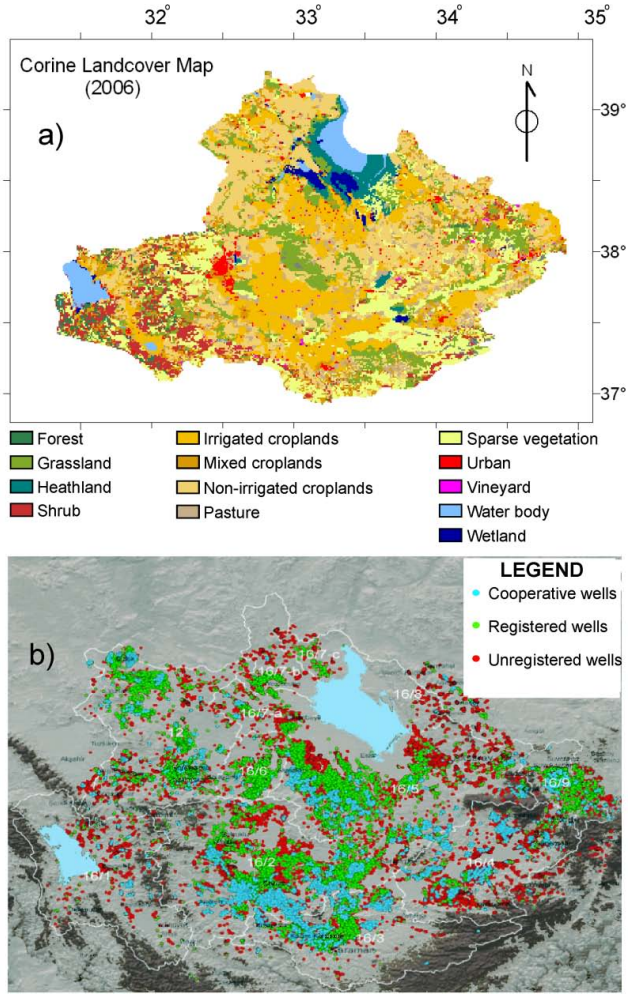


**Fig. 2. (a)** Corine land cover classification map of the Konya Basin (source: Ministry of Environment and Forestry); **(b)** distribution of the groundwater abstraction wells in and around the Konya Basin (source: unpublished data by State Hydraulic Works, DSI).

50 m depths. In the mountainous parts, forest and shrub lands form the dominant land cover. The distribution of agricultural crops (based on data from 2007) is as follows: 38 % cereals, 28 % sugar beet, 19 % vegetables, 13 % fruits and 2 % other (unpublished data from State Hydraulic Works, DSI).

Although surface water is also utilized, groundwater is the main source of water for irrigation. It can be accessed almost anywhere in the flat areas of the basin by means of 50 to 250 m deep wells (Bayari et al., 2009) abstracting from the Neogene aquifer. According to an unpublished inventory conducted by the regional water authority (DSI), there are more than 90 000 groundwater abstraction wells, around 75 % of which are unregistered, in the Konya Basin. The distribution of the groundwater abstraction wells is shown in Fig. 2b. Most of the wetlands and the water bodies in the region can also be classified as groundwater-dependent ecosystems.

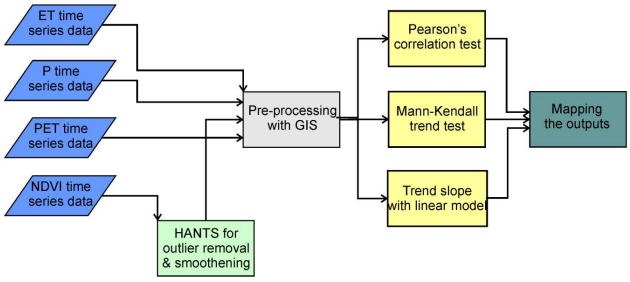


**Fig. 3.** Flowchart of trend analysis using satellite-based data sets.

## 2.2 Methods

A systematic framework is essential for detecting trends (Burn and Elnur, 2002). In this regard, we first established a consistent and spatiotemporally continuous time series of the variables, and then applied widely used statistical tests such as Mann–Kendall trend and Pearson's correlation tests and linear models to detect the significance, direction and magnitude of the trends and correlations. Figure 3 presents a flowchart of the analysis. The methods and the data sets are described below.

### 2.2.1 Harmonic analysis of time series

A harmonic analysis of time series (HANTS) algorithm was developed by Verhoef et al. (1996), which uses an iterative curve fitting starting with all data points and sequentially removing the pronounced negative outliers. Clouds always have a negative influence on the NDVI and therefore taking the maximum value of the NDVI over a limited period (i.e. maximum value compositing) tends to remove most cloud contaminated observations. The HANTS algorithm also removes the effect of clouds on the NDVI value, but by using an iterative curve fitting, that is, a least squares curve is estimated based on all data points, and the observations that have the greatest negative deviation from the curve therefore are removed first. Next a new curve is computed based on the remaining points and the process is repeated (Julien et al., 2006). Eventually the iteration leads to a smooth curve that approaches the upper envelope over the data points. As a result, more reliable estimates of yearly NDVI averages and first harmonic amplitudes and phases are achieved. The amplitude of the first harmonic indicates the variability of vegetation productivity over the year. The phase of the first harmonic summarizes the timing of vegetation green-up.

### 2.2.2 Trend and correlation analyses

The time series of all the hydrologic variables and vegetation greenness (NDVI) were analysed using the Mann–Kendall non-parametric test for trend. Mann (1945) originally used this test and Kendall (1975) subsequently derived the test statistic distribution. The Mann–Kendall test has two

parameters that are of importance for trend detection: the significance level that indicates the trend's strength ($p$ value), and the slope magnitude (Kendall's Tau) estimate that indicates the direction as well as the magnitude of the trend. After detecting the significance, direction and magnitude of trends by the Mann–Kendall test, the quantities (slopes) of trends are determined using linear models.

In order to apply the trend analysis in a spatially distributed manner, the Mann–Kendall test was applied using the R software and the Kendall package for R (http://cran.r-project.org/web/packages/Kendall/Kendall.pdf).

Pearson's correlation test ($r$) was applied to assess the correlations between the time series of different variables. The test has two key properties of magnitude and direction indicated by Pearson's $r$ value ranging between $-1$ and 1. Pearson's correlation test was applied using the R software and rcorr function of Hmisc package for R (http://cran.r-project.org/web/packages/Hmisc/Hmisc.pdf).

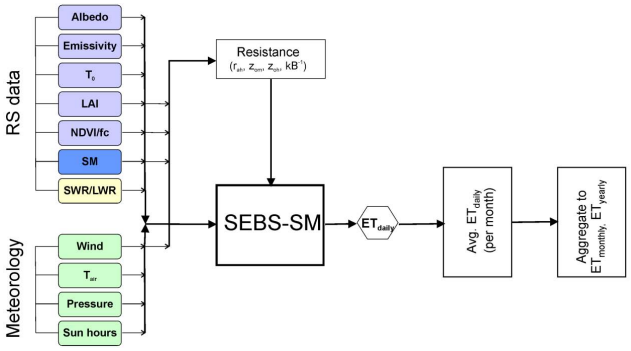


**Fig. 4.** Input data for SEBS-SM and flowchart for obtaining yearly ET (Adapted from Gokmen et al., 2013). In the figure, $T_0$: surface temperature, $T_{air}$: air temperature at reference height, LAI: leaf area index, NDVI/fc: normalized difference vegetation index/fraction of vegetation cover, SM: soil moisture, SWR/LWR: short-wave incoming radiation/long-wave incoming radiation, $r_{ah}$: aerodynamic resistance, $z_{0h}$: roughness height for heat, $z_{0m}$: roughness height for momentum, $kB^{-1}$: dimensionless excess resistance parameter.

## 2.3 Data

Table 1 provides a summary of the input data that were used to obtain the hydrological and vegetation variables for time series analysis. Our study covered the period between 2000 and 2010, which was mainly limited by the start of MODIS satellite observations. MODIS data are highly suitable for regional scale studies thanks to its moderate spatial (1 km) and high temporal (daily) resolutions, and formed the core data sets for ET and vegetation variables in this study. Further details of data and models that were used to obtain the time series of variables are described in the following sub-sections.

### 2.3.1 ET data

Nowadays RS-based surface energy balance models are increasingly used to determine the distribution of evapotranspiration from field to global scales. The physically based and single source SEBS model (Su, 2002) is one of the surface energy balance models widely used by the scientific community. SEBS estimates actual evapotranspiration (ET) using RS retrievals and meteorology data, and it has been applied in many regional to global studies (Gokmen et al., 2013; Ma et al., 2007, 2012; Pan et al., 2008, 2012; Vinukollu et al., 2011; Jin et al., 2009; Oku et al., 2007; Jia et al., 2003). The details of SEBS algorithm are provided in Su (2002) and Su et al. (2001).

In this study, we used a modified version of SEBS called SEBS-SM (Gokmen et al., 2012) for the estimation of the spatiotemporal distribution of actual evapotranspiration. The SEBS-SM (Gokmen et al., 2012) integrates soil moisture through incorporating a water stress index into the model for better accounting for moisture-limited evapotranspiration regime, which is typical in semi-arid regions. The performance of SEBS-SM was tested by Gokmen et al. (2012) through comparing it with ground data by Bowen ratio stations, and also through establishing a yearly water budget (Gokmen et al., 2013), and proved to be an overall improvement to the original model under water-stressed conditions. Gokmen et al. (2012) reported an overall relative error (rRMSE) of 26 % for SEBS-SM (which was originally 36 % for SEBS) according to the comparisons with observations from the Bowen ratio stations installed in in the Konya Basin. With respect to the yearly ET, SEBS-SM estimated a lower yearly ET than the original SEBS depending on the water-stress conditions. The magnitude of lowering by SEBS-SM was proportional to the aridity of the area (mean: $\sim -120$ mm, max: $\sim -400$ mm), and was better matching with the low yearly precipitation values in these areas (Gokmen et al., 2013).

Figure 4 provides a flowchart of obtaining the daily, monthly and yearly ET by SEBS-SM. The SEBS-SM was run on a daily interval for the study period (2000–2010). For filling the data gaps and obtaining monthly/yearly ET, we followed the methodology of Gokmen et al. (2013).

To retrieve the necessary input parameters for the model, we used MODIS land products (https://lpdaac.usgs.gov/products/modis_products_table) and AMSR-E and TRMM-TMI soil moisture products (Owe et al., 2008). As shown in Table 1, leaf area index (LAI) product of MODIS was available only after July 2002. For the missing LAI input data during 2000–2002, we used alternatively the formula by Wang et al. (2005) to estimate the LAI from NDVI. Furthermore, for soil moisture input data, we used AMSR-E and TRMM-TMI soil moisture products in combination, because AMSR-E product was available starting from June 2002. The use of two different data sets did not necessitate any intercalibration procedure because, as described in Gokmen et al. (2012) in detail, SEBS-SM utilizes the time series of soil

**Table 1.** The summary of the data used in the study.

| Variable | Input data | Source | Spatial resolution | Temporal resolution | Temporal coverage |
|---|---|---|---|---|---|
| Evapotranspiration | Albedo | MODIS | 500 m | 16-daily | 2000–2010 |
| | Emissivity | MODIS | 1000 m | Daily | 2000–2010 |
| | Land surface temperature | MODIS | 1000 m | Daily | 2000–2010 |
| | Leaf area index | MODIS | 1000 m | 8-daily | 2002–2010 |
| | NDVI | MODIS | 500 m | 16-daily | 2000–2010 |
| | Surface soil moisture | TRMM-TMI | ~25 km | 2–3 daily | 2000–2002 |
| | | AMSR-E | ~25 km | 2–3 daily | 2002–2010 |
| | Short-& long-wave radiation | ECMWF | ~75 km | Daily | 2000–2010 |
| | Wind | Meteo.station | Point data | Daily | 2000–2010 |
| | Air Temperature | Meteo.station | Point data | Hourly | 2000–2010 |
| | Pressure | Meteo.station | Point data | Daily | 2000–2010 |
| | Sunhours | Meteo.station | Point data | Daily | 2000–2010 |
| Precipitation | TRMM-precipitation | TRMM | ~25 km | Monthly | 2000–2010 |
| | Gauge-precipitation | Rain gauges | Point data | Monthly | 2000–2010 |
| Vegetation greenness | NDVI | MODIS | 500 m | 16-daily | 2000–2010 |
| Potential ET | Pan evaporation | Meteo.station | Point data | Daily | 2000–2010 |

moisture information as relative soil moisture (wetness) values that represent the water-stress conditions, and it is insensitive to absolute values of soil moisture.

In addition to the RS data, the necessary meteorological forcing data were obtained from the Turkish Meteorological Service for the 18 stations located in and around the basin (Fig. 1). The point measurements of the stations were spatially interpolated using the natural neighbour interpolation. With respect to instantaneous and daily air temperature, additionally, the local lapse rates were calculated for the mountainous areas and integrated (based on a DEM) in the interpolation of air temperature data. Finally, the down-welling short-wave and long-wave radiation flux ($R_{swd}$ and $R_{lwd}$), boundary layer height and dew point temperature at 2 m height were retrieved from the high-resolution gridded ECMWF (The European Centre for Medium-Range Weather Forecasts) interim reanalysis data set (http://data-portal.ecmwf.int/).

In addition to actual ET (denoted as ET) time series data, we also used the time series of potential evapotranspiration (PET) as an indicator of climate-related changes, because it is a representation of the atmospheric demand (e.g. changing radiation, or vapour-pressure deficit, which is often associated with temperature) for evapotranspiration. The spatiotemporal PET distribution of the Konya Basin was obtained using the class-A pan evaporation data from the 18 meteorological stations (Fig. 1) and the simplified formula by Snyder et al. (2005).

### 2.3.2 NDVI data

We used the MODIS NDVI product MOD13A1, which is designed to provide consistent spatial and temporal comparison of vegetation conditions. Global MOD13A1 gridded data are provided every 16 days (as 16-daily composite) at 500 m spatial resolution. This product is computed from atmospherically corrected bi-directional surface reflectances that have been masked for water, clouds, heavy aerosols, and cloud shadows. The accuracy of these MODIS Vegetation Indices has been assessed over a widely distributed set of locations and time periods via several ground-truth and validation efforts and they are ready for use in scientific publications (https://lpdaac.usgs.gov/products/modis_products_table/mod13a1).

Although the 16-daily composite NDVI product removes most of the cloudy pixels by selecting the highest value of NDVI during each 16-day period for each pixel, there can still be some remaining cloud contaminated pixels especially in regions experiencing long winter/wet season with continuous cloud casting. Therefore, we applied the HANTS algorithm for removing the effect of clouds on the NDVI value. Finally, we resampled the originally 0.5 km spatial resolution of MODIS NDVI product to 1 km resolution using bicubic interpolation in order to match it with the resolution of other variables.

### 2.3.3 Precipitation data

To establish the time series of the precipitation distribution, we used the monthly product of the Tropical Rainfall Measuring Mission (TRMM-3B43) combined with local rain gauge measurements. The TRMM algorithm combines 4 independent sources: (1) monthly average TMI (TRMM Microwave Imager) estimate, (2) monthly average SSM/I (Special Sensor Microwave Imager) estimate, (3) the pentad-average adjusted merged-infrared (IR) estimate, and (4) the monthly accumulated CAMS (Climate Assessment and Monitoring System) and GPCC (Global Precipitation Climatology Centre) rain gauge analysis. The monthly TRMM product has 25 km × 25 km spatial resolution. (http://gcmd.nasa.gov/KeywordSearch/Metadata.do).

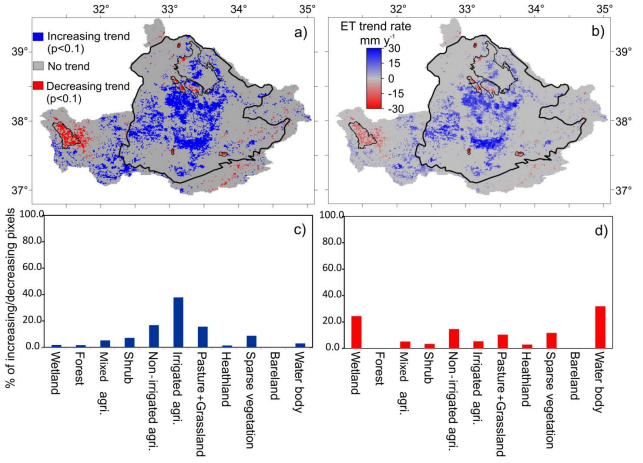


**Fig. 5.** The distributions of **(a)** significant trends, and **(b)** the magnitudes of the trends of yearly ET in the Konya Basin, and the histograms of the areas with **(c)** increasing trend, **(d)** decreasing trend for different land covers.

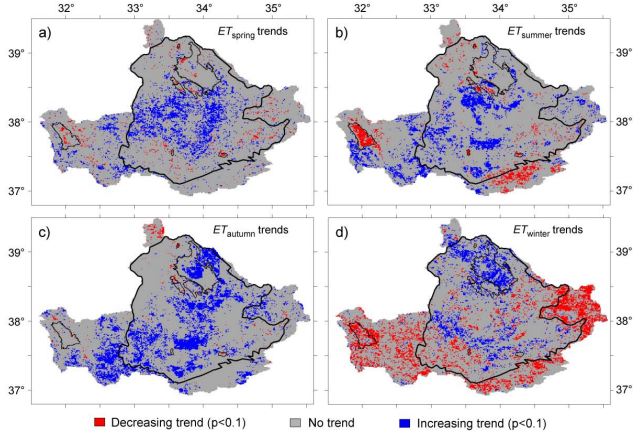


**Fig. 6.** Distributions of trends in the seasonal ET in the Konya Basin for **(a)** spring, **(b)** summer, **(c)** autumn, **(d)** winter between 2000 and 2010.

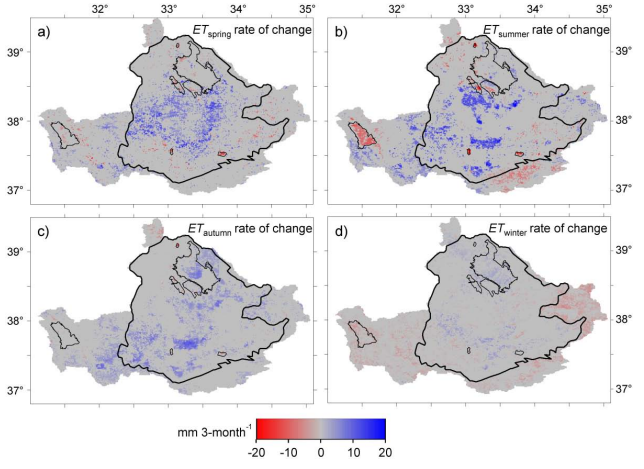


**Fig. 7.** The distributions of the magnitudes of the trends in the seasonal ET in the Konya Basin for **(a)** spring, **(b)** summer, **(c)** autumn, **(d)** winter.

Pan et al. (2008) indicated that TRMM products have large differences compared to ground observations at short time interval (3-hourly) but the discrepancies become smaller as the aggregation time increases. They also report a positive bias of the TRMM product. Similarly, Gokmen et al. (2013) compared the wet and dry season 6-monthly TRMM rainfall data with the gauge observations, and found a positive bias of around 80 mm by TRMM for the wet seasons in the Konya Basin. Therefore, we used a bias-removed time series of TRMM rainfall data based on the comparison by Gokmen et al. (2013). Although the TRMM data is available starting from 1998, we used a data set between the year 2000 and 2010 to be consistent with the other times series.

## 3 Results

### 3.1 ET trends

Figure 5a shows the distribution and direction of significant trends in the yearly ET in the Konya Basin. According to Fig. 5a, the areas with significant ($p < 0.1$) increasing yearly ET are much larger than the areas with decreasing trend, although the increasing trend is not basin-wide but spatially clustered in certain areas especially in the Konya plain part (inside the polygon). When we look at the rate of change (Fig. 5b), the highest increasing rates are observed in the Konya plain part and reach up to 30 mm yr$^{-1}$, which would mean more than 300 mm increase in the yearly ET during the study period (2000–2010). With respect to the distribution of the increasing ET areas over different land covers, Fig. 5c clearly shows that this trend mostly occurred in irrigated croplands, followed by non-irrigated croplands, pasture and grassland. In terms of decreasing trend of ET, Fig. 5a, b and d show that the decreasing trend occurred only in certain distinctive places (e.g. around Lake Beyşehir and the wetlands in the Konya plain indicated by smaller polygons), while the rate of decreasing trend was especially higher in the wetlands reaching around $-30$ mm yr$^{-1}$ (Fig. 5b).

Results of the seasonal ET trend analysis are shown in Figs. 6a–d and 7a–d. The distribution and direction of the trend (Fig. 6a–d), except for winter, shows generally a similar pattern as the yearly trend with a dominantly increasing trend especially in the plain part. The distribution was more spatially concentrated in the summer compared to more dispersed distribution in spring and autumn. Comparing the seasons the decreasing trend was largest in winter, especially in the mountainous part (outside the polygon). On the other hand, from the distribution of the rate of trend for each season (Figs. 7a–d) it is clear that the highest rate of change (both increasing and decreasing) among all seasons occurred in the

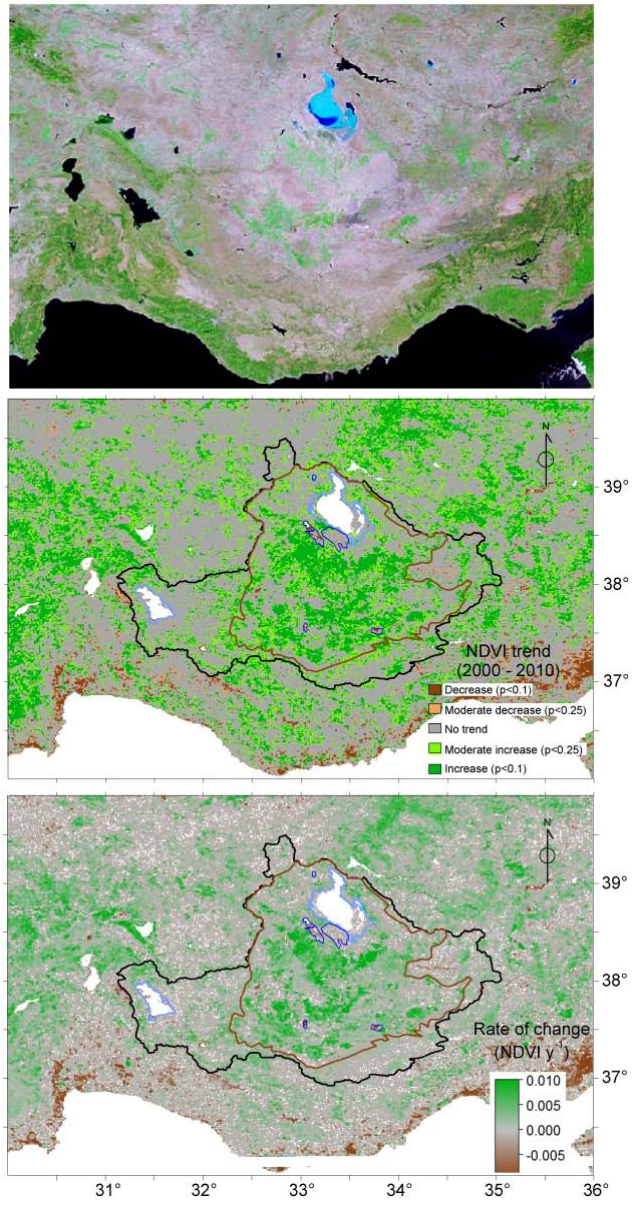


**Fig. 8. (a)** False-colour composite of MODIS image (RGB = bands 7, 2, and 1), **(b)** distribution of NDVI trends and, **(c)** magnitudes of the trends in the yearly average NDVI in and around the Konya Basin.

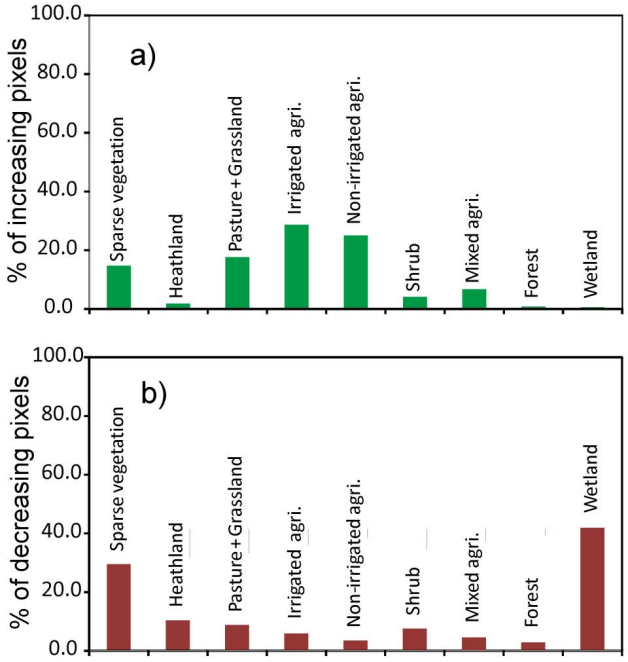


**Fig. 9.** The distribution of areas with **(a)** increasing trend, **(b)** decreasing trend in yearly average NDVI for different land covers in the Konya Basin.

summer, as can be expected, since this season has the highest atmospheric demand for evapotranspiration. On the opposite, the change of seasonal ET was lowest in winter (Fig. 7d), since the contribution of the winter ET to the overall yearly ET trend is the least among the seasons.

### 3.2 Trends in vegetation greenness

Figure 8 shows a false colour composite image and the distribution and the magnitudes of trends in the average yearly NDVI in and around the Konya Basin during the study period (2000–2010). Figure 8b reveals two different regional trends: a generally decreasing trend in the mountainous range along the Mediterranean coast in the south, while in the inner parts where continental climate prevails, increasing trend areas are generally observed including the Konya Basin, as indicated by the polygon. On the other hand, Fig. 8c indicates that the areas with the highest rates of increasing trend are observed in the Konya Basin (inside the polygon) with rates reaching around 0.01 NDVI $yr^{-1}$.

When we focus on the distribution of the average NDVI trends inside the Konya Basin (black-coloured polygon in Fig. 8b), we firstly observe that the increasing trend is mainly in the plain areas (inside the brown-coloured polygon) rather than in the mountainous parts (between black- and brown-coloured polygons). Furthermore, crossing the map of mean NDVI trends (Fig. 8b) with the land cover map (Fig. 2a), we found that the increasing trend of mean NDVI was mostly observed in irrigated and non-irrigated cropland covers, followed by the pasture and grassland land cover (Fig. 9a). On the other hand, Fig. 9b shows that the decreasing NDVI areas are mainly wetlands (small polygons) and sparse vegetation.

Lastly, Fig. 10a and b show the distribution of the trend and the rate of change in the amplitude of NDVI. Amplitude indicates the level of temporal variation in NDVI and high amplitude means a wide range of seasonal variation. Compared to the large areas with increasing trend for the mean NDVI (Fig. 8b), the areas with increasing trend of NDVI amplitude are smaller in the Konya plain (inside the

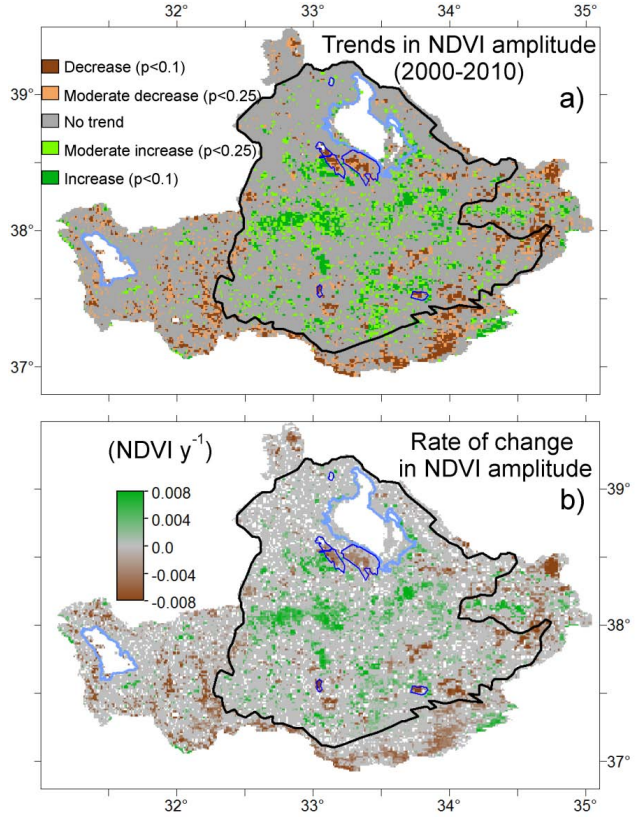


**Fig. 10. (a)** Distribution, and **(b)** magnitude of trends in the yearly amplitude of NDVI in the basin.

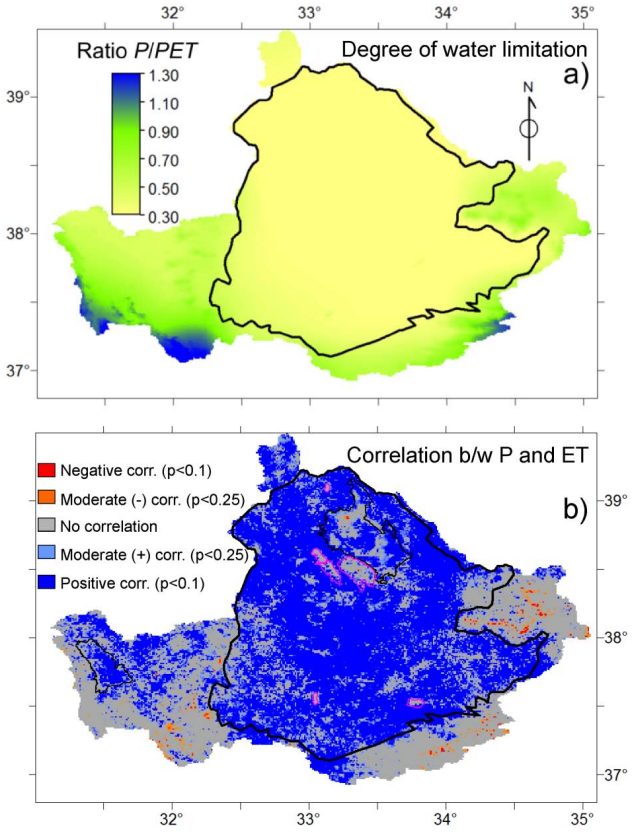


**Fig. 11.** The distribution of **(a)** water limitation **(b)** the correlation between $P$ and ET in the basin.

black-coloured polygon). These areas are mainly related to the increase in the maximum NDVI values due to intensification of irrigation and land cover changes. With respect to the decreasing trend in the NDVI amplitudes, those are observed in the wetlands (dark-blue coloured polygons) and also in the mountainous parts (outside the black polygon – mostly shrub and forest land covers), which can be related to the either decreasing NDVI maximum values or increasing NDVI minimum values. With respect to the rate of change in NDVI amplitude, Fig. 10b shows that highest rate of increasing or decreasing amplitudes were localized in some parts of the basin instead of a general homogeneous spread.

### 3.3 Partitioning of the anthropogenic effects from the climate-driven changes in ET trends

To be able to attribute the causes of ET trends and their distribution, it is first needed to reveal the distribution of the controlling mechanisms of ET (i.e. energy demand and moisture supply) (Teuling et al., 2009). Figure 11a shows the distribution of the degree of water limitation given by the criterion of Parsons and Abrahams (1994) who defined the water-limited environments as the areas having a $P$ PET$^{-1}$ ratio less than 0.75. We can conclude that except for the upstream mountainous parts in the southwest, south and east, the whole Konya plain (indicated by the polygon in Fig. 11a) can be classified as highly water-limited environment with a $P$ PET$^{-1}$ ratio of about 0.3. Additionally, we assessed the correlation between the $P$and ET using Pearson's correlation test: Figure 11b not only confirms the general pattern provided by $P$ PET$^{-1}$ map (Fig. 11a) about the division of moisture supply/energy demand control of ET between Konya plain and mountainous parts, respectively, but also indicates some patches of energy-limited areas in the Konya plain despite the low precipitation input ("no correlation" areas in Fig. 11b). This can be partly related to additional groundwater discharge to the wetlands (smaller polygons indicated by purple colour) and water bodies (e.g. hyper-saline Tuz Lake in the north), which show that these ecosystems are more groundwater- than precipitation-dependent to sustain high evapotranspiration rates. Apart from these naturally groundwater-fed areas, the other energy-limited areas in the Konya plain mostly correspond to irrigated croplands where additional water supply (mainly from groundwater) is provided to sustain the crop water requirements.

To reveal further the causes of ET trends in the Konya Basin, Fig. 12a–d show the distributions of the significance and rate of trends in the climate-related variables of potential evapotranspiration (PET) and precipitation ($P$). According

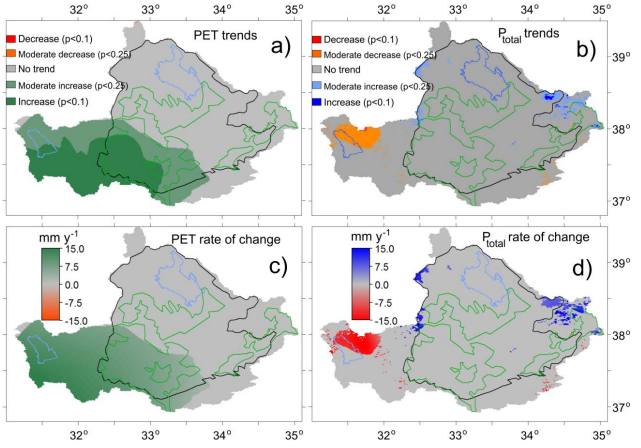


**Fig. 12. (a)** The distribution and direction of PET trends, **(b)** the distribution and direction of $P$ trends **(c)** the magnitude of PET trends, **(d)** the magnitude of $P$ trends. The black polygon shows the water-limited part, the green polygons indicate the irrigated croplands and the blue polygons the lakes.

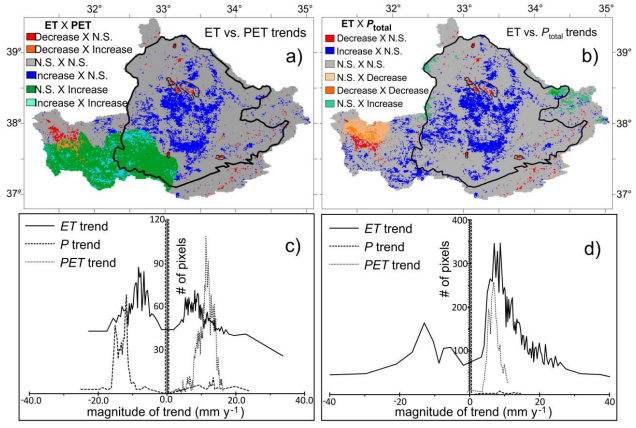


**Fig. 13. (a)** The cross relation between ET vs. PET trends, **(b)** cross relation between ET vs. PET trends (Note that "N.S." represent "Not significant trend" in the legends of Fig. 13a and b), **(c)** histograms of ET, PET and $P$ trends for the energy-limited part (outside Konya-plain polygon), **(d)** histograms of ET, PET and $P$ trends for the water-limited part (inside Konya-plain polygon). Note that the histograms of all the three variables represents the represents the areas with significant ET trend ($p < 0.25$) both in the energy- and water-limited parts.

to Fig. 12a, PET has an increasing trend in the southwest of the basin, which includes the mountainous upstream part and the southwest corner of the Konya plain (green areas inside the black polygon). In terms of rate of PET trend (Fig. 12c), the increasing trend reaches to 15 mm yr$^{-1}$ in the mountainous part and gradually decreasing towards the inner plain part. Note that the PET map is an interpolation result of point data (see Sect. 2.3.1), so the level of spatial detail is coarser than the satellite-image-based maps, that is, $P$ and ET. With respect to precipitation (Fig. 12b), there was only some small patches of areas which had moderate ($p < 0.25$) decreasing and increasing trends in the west (in and around lake Beysehir) and east of the basin, respectively. In these patches, the rates of decreasing and increasing trends were around 10–15 mm yr$^{-1}$.

Finally to be able to partition quantitatively the causes of ET trends between anthropogenic (e.g. irrigation) and climate drivers (i.e. $P$ and PET), Fig. 13a–b firstly show the cross maps of ET versus PET and $P$ trends, respectively. Overlaying the trend distributions of ET and PET, we can observe that most of the areas with significant ET increase and decrease (dark blue and red colours, respectively) in the Konya plain (water-limited part) had no significant trend of PET ($p < 0.1$). Similarly, the combined distribution of ET and $P$ trends in Fig. 13b shows that, especially in the Konya plain part, neither the increasing nor the decreasing trends of ET had relation with the changes in $P$ because there was no significant trend of $P$ in any direction in these areas. The only part $P$ and ET trends had correlation was around lake Beysehir in the west (brown colour), where both ET and $P$ had decreasing trends, where ET had been depicted as relatively moisture limited (i.e. positively correlated with precipitation) in Fig. 11a and b. More specifically, Fig. 13c–d show the histograms of ET, PET, and $P$ trends in the areas with significant ET trend for energy and water-limited regions separately. Based on these histograms, Table 2 presents the quantitative summary of attributing and partitioning of ET trends in the energy- and water-limited parts. According to Table 2, in the water-limited part, for a total ET increase of about 135 MCM yr$^{-1}$ (mainly croplands, Fig. 5c), only about 21 MCM yr$^{-1}$, which corresponds to about 16 % of total ET increasing trend, can be attributed to the increasing trend of PET in these areas, while the rest cannot be explained by PET or $P$ trends. With respect to the decreasing trend areas of ET, neither PET nor $P$ trend can explain any of the ET decrease, which is totally about $-25$ MCM yr$^{-1}$ (mainly in the wetlands and water bodies, Fig. 5d) in the water-limited part. On the other hand, in the energy limited part, the whole of the ET increasing trend (i.e. about 25 MCM yr$^{-1}$) can be explained by the increasing PET trend of totally 44 MCM yr$^{-1}$. While for the decreasing portion of ET in the energy limited part (i.e. about $-13$ MCM yr$^{-1}$), 65 % of it can be explained by the decreasing trend of $P$ (i.e. about $-9$ MCM yr$^{-1}$).

Based on Figs. 12, 13 and Table 2, we can conclude that the ET trends that occurred in the Konya plain, where moisture supply controls the ET regime, are mostly (about 84 % of the increase and 100 % of the decrease) not related to the changes in the climate variables such as $P$ and PET. Hence, the ET trends in the plain can mainly be attributed to the anthropogenic effects, such as land and water use changes (i.e. conversion of lands to the irrigated croplands and intensification of groundwater irrigation), which is also supported by NDVI trends of these land cover types (Figs. 8b and 9a). On

**Table 2.** The quantitative summary of ET, PET and $P$ trends for the areas with significant ET trend ($p < 0.25$) in the energy- and water-limited parts, separately.

| | | | ET | PET | $P_{total}$ |
|---|---|---|---|---|---|
| Water-limited part | Increase | Avg. (mm yr$^{-1}$) | 13,6 | 6.8 | 10,9 |
| | | Total (MCM yr$^{-1}$) | 135,8 | 21.3 | 0,5 |
| | Decrease | Avg. (mm yr$^{-1}$) | −13,8 | −0,3 | 0,0 |
| | | Total (MCM yr$^{-1}$) | −12,2 | −0,006 | 0,0 |
| Energy limited part | Increase | Avg. (mm yr$^{-1}$) | 7.9 | 8.4 | 13,4 |
| | | Total (MCM yr$^{-1}$) | 24,8 | 44.3 | 1,1 |
| | Decrease | Avg. (mm yr$^{-1}$) | −6,3 | 0,0 | −13,2 |
| | | Total (MCM yr$^{-1}$) | −13.3 | 0,0 | −8,6 |

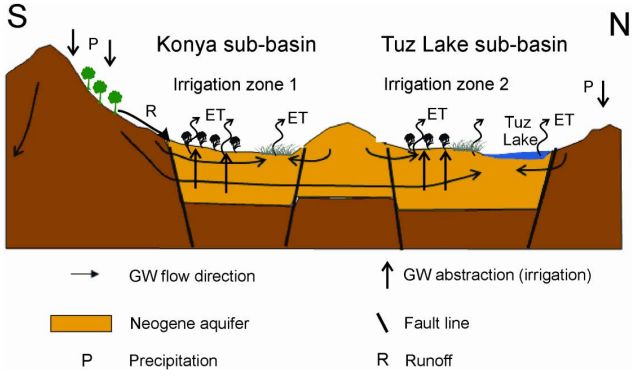


**Fig. 14.** The conceptual model of the Konya Basin (adapted from Gokmen et al., 2013).

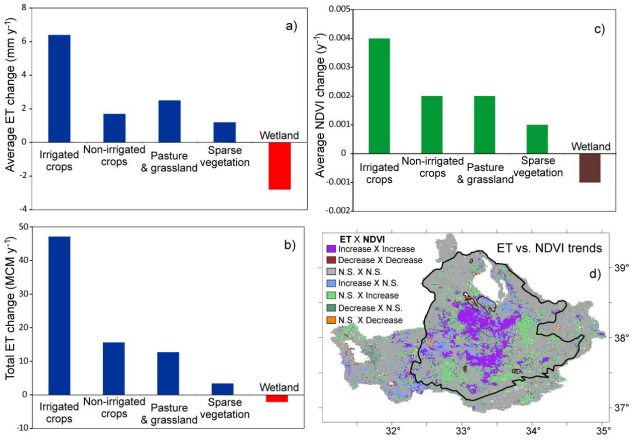


**Fig. 15.** The histograms of **(a)** average, **(b)** total ET changes and **(c)** average NDVI changes in the areas having significant trend (for $p <$ 0.1 significance level), **(d)** the distribution of the overlaid trends of ET and NDVI in the Konya plain during the study period (2000–2010).

the other hand, the ET trends that occurred in the mountainous part, especially in the southwest, are mainly related to the climate-related PET and $P$ trends.

### 3.4 Interactions between the water use (irrigation) and ecosystems (wetlands) health

In the Konya Basin, groundwater is the main source of water for irrigation (about 80 % according to Gokmen et al., 2013), because it can be accessed almost anywhere in the flat areas of the basin (Bayari et al., 2009). The conceptual diagram (Fig. 14), shows that the regional groundwater flow, from the mountains in the south towards the terminal Tuz Lake in the north, discharges at some wetlands and water bodies around the basin and sustains the ecosystems. As these groundwater-dependent ecosystems are highly sensitive to groundwater level changes, they are also directly affected by the agricultural activities that utilize groundwater as a source for irrigation.

Figure 15a and b show the changes in the average and total volume of ET per year for different land cover classes in the water-limited Konya plain, which experienced mainly human-induced trends as shown in Sect. 3.3. According to Fig. 15a, irrigated croplands had the highest average increase of ET with 6.4 mm yr$^{-1}$, while the only decrease of ET was for wetland with a rate of −2.8 mm yr$^{-1}$. With respect to the changes in the total volumes of water evaporated in the areas having significant trends ($p < 0.1$), irrigated croplands was again leading with a totally 47.1 MCM yr$^{-1}$ increase of ET (which means more than 500 MCM increase of ET overall during 2000–2010 study period), followed by non-irrigated croplands with a total increasing volume of 15.6 MCM yr$^{-1}$. On the other hand, wetlands had a total decreasing volume of −2.1 MCM yr$^{-1}$, which adds up to about −23 MCM overall during 2000–2010 study period.

Moreover, showing the histogram of changes in the yearly average NDVI for different land covers, Fig. 15c indicates a similar distribution to Fig. 15a that the highest increasing rate of NDVI was observed for irrigated croplands (0.004 NDVI yr$^{-1}$), while the only decreasing rate was observed for

wetlands again ($-0.001$ NDVI yr$^{-1}$). Finally, Fig. 15d shows the overlaid distributions of both ET and NDVI to analyse if their trends also spatially correspond to each other. Figure 15d indicates that there is generally a good agreement for both significant increasing (purple colour) and decreasing (dark brown colour) trend areas, which suggest the drying trend of wetlands in the Konya plain is the direct result of the increasing rate of evapotranspiration from the croplands because the increasing irrigation water use is depleting the groundwater resources, upon which the wetlands are dependent on.

## 4 Discussion

Putting forward a regional perspective on the trends in evaporation, Teuling et al. (2009) stated that identifying the trends in evapotranspiration (and hence runoff) can only be understood regionally (and temporally) because the controlling mechanisms of ET (i.e. energy demand and moisture supply) vary from region to region. In addition, Douville et al. (2012) state that, among the water cycle components, changes in ET are easier to detect and attribute than changes in precipitation or runoff given their stronger signal-to-noise ratio, because precipitation and runoff are intermittent and non-linear processes whereas ET occurs every day and is much better time integrator of regional change (climate, land and water use, among others). Therefore, following a regional perspective, we used the time series of RS-based ET estimations as the key variable to assess the distribution of the ecohydrological changes in the semi-arid Konya Basin.

Detection of trends and their significance with confidence generally requires consistent and long-term records of variables considered, especially in the case of detecting climate change driven trends. In this respect, 11 yr period (2000–2010) of this study, which was mainly limited by the availability of one of the core data set (i.e. MODIS), was relatively short especially for assessing the climate-related trends. However, some human-induced trends, such as land-use changes, are likely to have an important role regionally (Jung et al., 2010) and can be detected in relatively short periods as revealed by a previous study by Rodell et al. (2009) about the satellite-based estimates of groundwater depletion in India during six years study period. Similarly, presenting a striking example of a semi-arid region where anthropogenic factors (i.e. land-use changes and non-sustainable groundwater use) strongly affect the hydrological fluxes and ecosystems health, our study could reveal the human-induced trends in the ecohydrology of the region in a relatively short period of about a decadal timescale (2000–2010). However, in case of applying such a framework for regions not subjected to strong human influences, one must pay special attention to the length of data that allow the detection of trends with high statistical confidence (i.e. detection time). As stated by Leroy et al. (2008), it is obvious that the longer the time series, the easier it should be to distinguish a trend from natural variability (and measurement uncertainty), because shorter periods of record generally have small signal-to-noise (S / N) ratios (Allen et al., 1994). The strong timescale dependence of S / N ratios arises primarily because of the large decrease in noise amplitude as the period used for trend fitting increases (Santer et al., 2011). Based on a hypothetical data set with certain statistical characteristics, Leroy et al. (2008) determined the minimum detection time as about 33 yr for detecting a global warming signal of 0.2 K decade$^{-1}$. Similarly, assessing the trend consistency over a range of timescales (from 10 to 32 yr), Santer et al. (2011) states that multi-decadal records are required for identifying the human effect on the climate variables (e.g. temperature) with high statistical confidence.

To ensure a reliable assessment of the ecohydrological trends in a relatively short study period in the region, we employed an integrated trend analysis of the ET time series along with the time series of NDVI as the indicator of vegetation greenness, and $P$ and PET as the representatives of climate-related changes so that we could evaluate the consistencies between hydrological and vegetation trends and attribute the observed trends to climate and/or anthropogenic effects. Assessing the multi-decadal changes in surface soil moisture globally, Dorigo et al. (2012) not only merged different soil moisture products from different satellite sensors but also compared the observed trends with trends in a precipitation data set, and a vegetation data set in order to identify consistencies and potential shortcomings. Our combined assessment of the trends in ET and NDVI time series (2000–2010) revealed that hydrological and vegetation trends were consistent with each other: significant ($p < 0.1$) increasing trends were mainly in the croplands (Figs. 5c and 9a), while the significant decreasing trends ($p < 0.1$) were mostly in wetlands (Figs. 5d and 9b). Furthermore, according to the comparison with the trends in climate-related $P$ and PET time series it was revealed that the observed ecohydrological trends (i.e. ET and NDVI) in the basin, especially in the water-limited plain part, were not related to the climate-related variables (Figs. 12 and 13) except for only about 16 % of the increasing ET trend being explained by the increasing trend of PET (Table 2). The emerging picture suggests that the greening trend of the vegetation in the Konya plain is mostly related to land cover changes (i.e. conversion into irrigated croplands) and to the intensification of the irrigated agricultural activities, which in turn caused drying out of some of the wetlands and the natural vegetation which mostly depend on the groundwater, the main source of irrigation water as well. These findings are also in agreement with the previous studies by Bayari et al. (2009) and Gokmen et al. (2013), who reported groundwater depletion due to supplementary irrigation to sustain the agricultural activities in the region.

With respect to the possible sources of errors in the analysis, it should be noted that the CORINE land cover map (Fig. 2a) used in analysing the distribution of trends among

different land cover types was from 2006 (source: Ministry of Environment and Forestry of Turkey), rasterized originally from a polygon map and resampled to 1 km$^2$ resolution. Firstly, especially for croplands with fields of varying sizes, conversion from the polygon map (with a smallest mapping unit of about 0.001 km$^2$) to such a medium-scale pixel resolution (1 km$^2$) is vulnerable to the mixed-pixel effect, which can affect the distribution of ET trends among the land covers. Although irrigated croplands can be clearly identified with their increasing ET and NDVI trends in the Konya plain (Figs. 5c, 9a, 14a–c), some considerable increasing trends were also observed for pixels, which are indicated on the maps as non-irrigated croplands and pasture/grassland mostly on the edges of irrigated regions. Since no climate-related trends were observed in the plain during the study period, the increasing ET and NDVI in these land cover types can be partly explained by the mixed-pixel effect, that is, there are patches of irrigated lands within non-irrigated pixels. Secondly, as the land cover map is only representative for the year 2006, it is not fully representative for all changes of land cover that have occurred in the Konya plain. Hence, although shown as increasing trends in non-irrigated croplands and pasture in the figures (Figs. 5c, 9a and 15a–c), it is likely that part of these areas were already fully converted into irrigated croplands.

In addition, as the distribution of potential evapotranspiration (PET) was obtained from the point-base pan-A evaporation data of 18 meteorology stations (Fig. 1), there is certain errors attached to the interpolation of the point-based data. According to the inter-comparison of the results by the original point-base data and the interpolated map, the significance/signs of trends agreed on all the stations except two (i.e. Konya and Nigde stations in Fig. 1), and quantitatively, the spatial average of the PET increasing trend by the interpolated map was about 4.5 mm lower than the average of the stations that had significant increasing trend. In all, such a difference of PET would cause an additional total PET of about 15 MCM in the significant change areas (in both energy- and water-limited parts), which would still correspond to less than 10 % the total ET increase in these areas (Table 2).

## 5 Conclusions

In this study, we analysed the recent trends (from year 2000 to 2010) in evapotranspiration, vegetation greenness (i.e. NDVI) and precipitation using satellite-based observations to assess the human-induced changes in the hydrology and the associated ecological health of the semi-arid Konya closed basin where both human activities (agriculture) and natural ecosystems are highly groundwater dependent.

Based on our relatively finer scale (1 km) analysis of the spatiotemporal trends, we conclude that the controlling mechanisms of ET even spatially vary inside the region. Therefore, for better assessment of the trends, it is necessary to analyse the spatial distribution of controlling regimes together with trends of ET, also at sub-regional scale.

In arid and semi-arid regions, ET is the main and frequently the only outflux from the hydrological system, hence it can be considered one of the key variables to understand the regional ecohydrological changes and trends, especially when driven by anthropogenic causes. We showed that an integrated trend analysis of consistently established ET time series along with vegetation (NDVI) and climate variables (i.e. PET, $P$) is effective to reveal the distribution and quantity of human-induced changes in the hydrology and the ecology of the semi-arid Konya Basin, where previous studies (Gokmen et al., 2013; Bayari et al., 2009) had also indicated huge non-renewable groundwater abstraction for irrigation, and corresponding groundwater head declines. The integrated assessment of hydrological (ET), vegetation (NDVI) and climate ($P$ and PET) variables not only better enable one to identify the consistencies among them but also better separate the climate-driven and human-induced trends spatially in the region.

Finally, our study presented an example of the utility of spatially and temporally continuous RS data in assessing the regional trends in hydrological and ecological variables and their interactions in a spatially distributed manner in a semi-arid region, which can also be adapted to other regions. Such spatiotemporally distributed analyses at the basin and regional level is particularly important considering that most of the water management interventions also take place at these scales.

*Acknowledgements.* We thank to Maciek W. Lubczynski for his support and valuable discussions about the research, especially regarding the groundwater related issues.

We thank to Hasan Z. Sarıkaya for his support for the realization of the research, especially with regards to field studies.

We also thank to the staff of Regional Water Authority (DSI 4. Bölge Müdürlüğü), especially to Mehmet Demirel, Kemal Olgun, and Adnan Başaran for their help in establishing the Bowen ratio stations and providing the ground data.

Finally, we thank to the editor handling the manuscript and the two anonymous reviewers for their constructive comments to improve this manuscript.

Edited by: J. Liu

## References

Alcaraz-Segura, D., Liras, E., Tabik, S., Paruelo, J., and Cabello, J.: Evaluating the Consistency of the 1982–1999 NDVI Trends in the Iberian Peninsula across Four Time-series Derived from the AVHRR Sensor: LTDR, GIMMS, FASIR, and PAL-II, Sensors, 10, 1291–1314, 2010.

Allen, M. R., Mutlow, C. T., Blumberg, G. M. C., Christy, J. R., McNider, R. T., and Llewellyn-Jones, D. T.: Global change detection, Nature, 370, 24–25, 1994.

Alsdorf, D. E. and Lettenmaier, D. P.: Tracking fresh water from space, Science, 301, 1491–1494, 2003.

Bayari, C. S., Ozyurt, N. N., and Kilani, S.: Radiocarbon age distribution of groundwater in the Konya Closed Basin, central Anatolia, Turkey, Hydrogeol. J., 17, 347–365, 2009.

Beck, H. E., McVicar, T. R., van Dijk, A., Schellekens, J., de Jeu, R. A. M., and Bruijnzeel, L. A.: Global evaluation of four AVHRR-NDVI data sets: Intercomparison and assessment against Landsat imagery, Remote Sens. Environ., 115, 2547–2563, 2011.

Burn, D. H. and Elnur, M. A. H.: Detection of hydrologic trends and variability, J. Hydrol., 255, 107–122, 2002.

Dorigo, W., de Jeu, R., Chung, D., Parinussa, R., Liu, Y., Wagner, W., and Fernandez-Prieto, D.: Evaluating global trends (1988–2010) in harmonized multi-satellite surface soil moisture, Geophys. Res. Lett., 39, L18405, doi:10.1029/2012GL052988, 2012.

Douville, H., Ribes, A., Decharme, B., Alkama, R., and Sheffield, J.: Anthropogenic influence on multidecadal changes in reconstructed global evapotranspiration, Nat. Clim. Change, 3, 59–62, 2012.

Du, J., He, F., Zhang, Z., and Shi, P. J.: Precipitation change and human impacts on hydrologic variables in Zhengshui River Basin, China, Stoch. Environ. Res. Risk Assess., 25, 1013–1025, 2011.

Evans, J. and Geerken, R.: Discrimination between climate and human-induced dryland degradation, J. Arid Environ., 57, 535–554, 2004.

Famiglietti, J. S., Lo, M., Ho, S. L., Bethune, J., Anderson, K. J., Syed, T. H., Swenson, S. C., de Linage, C. R., and Rodell, M.: Satellites measure recent rates of groundwater depletion in California's Central Valley, Geophys. Res. Lett., 38, L03403, doi:10.1029/2010GL046442, 2011.

Fan, Y., Li, H., and Miguez-Macho, G.: Global patterns of groundwater table depth, Science, 339, 940–943, 2013.

Fensholt, R. and Proud, S. R.: Evaluation of Earth Observation based global long term vegetation trends – Comparing GIMMS and MODIS global NDVI time series, Remote Sens. Environ., 119, 131–147, 2012.

Fensholt, R. and Rasmussen, K.: Analysis of trends in the Sahelian "rain-use efficiency" using GIMMS NDVI, RFE and GPCP rainfall data, Remote Sens. Environ., 115, 438–451, 2011.

Fensholt, R., Langanke, T., Rasmussen, K., Reenberg, A., Prince, S. D., Tucker, C., Scholes, R. J., Le, Q.B., Bondeau, A., Eastman, R., Epstein, H., Gaughan, A. E., Hellden, U., Mbow, C., Olsson, L., Paruelo, J., Schweitzer, C., Seaquist, J., and Wessels, K.: Greenness in semi-arid areas across the globe 1981–2007 – an Earth Observing Satellite based analysis of trends and drivers, Remote Sens. Environ., 121, 144–158, 2012.

Fontugne, M., Kuzucuoglu, C., Karabiyikoglu, M., Hatte, C., and Pastre, J. F.: From Pleniglacial to Holocene: a C-14 chronostratigraphy of environmental changes in the Konya Plain, Turkey, Quaternary Sci. Rev., 18, 573–591, 1999.

Gleeson, T., VanderSteen, J., Sophocleous, M. A., Taniguchi, M., Alley, W. M., Allen, D. M., and Zhou, Y. X.: Groundwater sustainability strategies, Nat. Geosci., 3, 378–379, 2010.

Gokmen, M., Vekerdy, Z., Verhoef, A., Verhoef, W., Batelaan, O., and van der Tol, C.: Integration of soil moisture in SEBS for improving evapotranspiration estimation under water stress conditions, Remote Sens. Environ., 121, 261–274, 2012.

Gokmen, M., Vekerdy, Z., Lubczynski, M. W., Timmermans, J., Batelaan, O., and Verhoef, W.: Assessing groundwater storage changes using RS-based evapotranspiration and precipitation at a large semi-arid basin scale, J. Hydrometeorol., doi:10.1175/JHM-D-12-0156.1, online first, 2013.

Grafton, R. Q., Pittock, J., Davis, R., Williams, J., Fu, G., Warburton, M., Udall, B., McKenzie, R., Yu, X., Che, N., Connell, D., Jiang, Q., Kompas, T., Lynch, A., Norris, R., Possingham, H., and Quiggin, J.: Global insights into water resources, climate change and governance, Nat. Clim. Change, 3, 315–321, 2013.

Hatzianastassiou, N., Katsoulis, B., Pnevmatikos, J., and Antakis, V.: Spatial and temporal variation of precipitation in Greece and surrounding regions based on global precipitation climatology project data, J. Climate, 21, 1349–1370, 2008.

Heumann, B. W., Seaquist, J. W., Eklundh, L., and Jonsson, P. AVHRR derived phenological change in the Sahel and Soudan, Africa, 1982–2005, Remote Sens. Environ., 108, 385–392, 2007.

Jia, L., Su, Z. B., van den Hurk, B., Menenti, M., Moene, A., De Bruin, H. A. R., Yrisarry, J. J. B., Ibanez, M., and Cuesta, A.: Estimation of sensible heat flux using the Surface Energy Balance System (SEBS) and ATSR measurements, Phys. Chem. Earth, 28, 75–88, 2003.

Jin, X. M., Schaepman, M. E., Clevers, J., and Su, Z. B.: Impact and consequences of evapotranspiration changes on water resources availability in the arid Zhangye Basin, China, Int. J. Remote Sens., 30, 3223–3238, 2009.

Julien, Y., Sobrino, J. A., and Verhoef, W.: Changes in land surface temperatures and NDVI values over Europe between 1982 and 1999, Remote Sens. Environ., 103, 43–55, 2006.

Jung, M., Reichstein, M., Ciais, P., Seneviratne, S. I., Sheffield, J., Goulden, M. L., Bonan, G., Cescatti, A., Chen, J. Q., de Jeu, R., Dolman, A. J., Eugster, W., Gerten, D., Gianelle, D., Gobron, N., Heinke, J., Kimball, J., Law, B. E., Montagnani, L., Mu, Q. Z., Mueller, B., Oleson, K., Papale, D., Richardson, A. D., Roupsard, O., Running, S., Tomelleri, E., Viovy, N., Weber, U., Williams, C., Wood, E., Zaehle, S., and Zhang, K.: Recent decline in the global land evapotranspiration trend due to limited moisture supply, Nature, 467, 951–954, 2010.

Karami, E. and Hayati, D.: Rural Poverty and Sustainability: The Case of Groundwater Depletion in Iran. Asian Journal of Water, Environ. Pollut., 2, 51–61, 2005.

Kendall, M. G.: Rank Correlation Methods, Charles Griffin, London, 1975.

Konikow, L. F. and Kendy, E.: Groundwater depletion: A global problem, Hydrogeol. J., 13, 317–320, 2005.

Lebel, T. and Ali, A.: Recent trends in the Central and Western Sahel rainfall regime (1990–2007), J. Hydrol., 375, 52–64, 2009.

Leroy, S. S., Anderson, J. G., and Ohring, G.: Climate Signal Detection Times and Constraints on Climate Benchmark Accuracy Requirements, J. Climate, 21, 841–846, doi:10.1175/2007JCLI1946.1, 2008.

Liu, J. and Yang, H.: Spatially explicit assessment of global consumptive water uses in cropland: green and blue water, J. Hydrol., 384, 187–197, 2010.

Liu, J., Folberth, C., Yang, H., Röckström, J., Abbaspour, K., and Zehnder, A. J. B.: A Global and Spatially Explicit Assessment of Climate Change Impacts on Crop

Production and Consumptive Water Use, PLoS ONE, 8, e57750, doi:10.1371/journal.pone.0057750, 2013.

Ma, W. Q., Hafeez, M., Rabbani, U., Ishikawa, H., and Ma, Y. M.: Retrieved actual ET using SEBS model from Landsat-5 TM data for irrigation area of Australia, Atmos. Environ., 59, 408–414, 2012.

Ma, Y. M., Song, M. H., Ishikawa, H., Yang, K., Koike, T., Jia, L., Meneti, M., and Su, Z. B.: Estimation of the regional evaporative fraction over the Tibetan Plateau area by using Landsat-7 ETM data and the field observations, J. Meteorol. Soc. Jpn, 85A, 295–309, 2007.

Mann, H. B.: Nonparametric Tests against Trend, Econometrica, 13, 245–259, 1945.

McGuire, V.: Changes in water levels and storage in the High Plains aquifer, predevelopment to 2007, USGS Fact Sheet, US Geological Survey Scientific Investigations Report, 2009–3005, 2009.

Milliman, J. D., Farnsworth, K. L., Jones, P. D., Xu, K. H., and Smith, L. C.: Climatic and anthropogenic factors affecting river discharge to the global ocean, 1951–2000, Global Planet. Change, 62, 187–194, 2008.

Morrow, E., Mitrovica, J. X., and Fotopoulos, G.: Water Storage, Net Precipitation, and Evapotranspiration in the Mackenzie River Basin from October 2002 to September 2009 Inferred from GRACE Satellite Gravity Data, J. Hydrometeorol., 12, 467–473, 2011.

New, M., Todd, M., Hulme, M., and Jones, P.: Precipitation measurements and trends in the twentieth century, Int. J. Climatol., 21, 1899–1922, 2001.

Oku, Y., Ishikawa, H., and Su, Z. B.: Estimation of land surface heat fluxes over the Tibetan Plateau using GMS data, J. Appl. Meteorol. Climatol., 46, 183–195, 2007.

Owe, M., de Jeu, R., and Holmes, T.: Multisensor historical climatology of satellite-derived global land surface moisture, J. Geophys. Res.-Earth, 113, 2003–2012, 2008.

Pan, M., Wood, E. F., Wojcik, R., and McCabe, M. F.: Estimation of regional terrestrial water cycle using multi-sensor remote sensing observations and data assimilation, Remote Sens. Environ., 112, 1282–1294, 2008.

Pan, M., Sahoo, A. K., Troy, T. J., Vinukollu, R. K., Sheffield, J., and Wood, E. F.: Multisource Estimation of Long-Term Terrestrial Water Budget for Major Global River Basins, J. Climate, 25, 3191–3206, 2012.

Parsons, A. J. and Abrahams, A. D. (Eds.): Geomorphology of desert environments, CRC Press, London, 1994.

Rodell, M., Chen, J. L., Kato, H., Famiglietti, J. S., Nigro, J., and Wilson, C. R.: Estimating groundwater storage changes in the Mississippi River basin (USA) using GRACE, Hydrogeol. J., 15, 159–166, 2007.

Rodell, M., Velicogna, I., and Famiglietti, J. S.: Satellite-based estimates of groundwater depletion in India, Nature, 460, 999–1002, 2009.

Ryu, Y., Baldocchi, D. D., Ma, S., and Hehn, T.: Interannual variability of evapotranspiration and energy exchange over an annual grassland in California, J. Geophys. Res.-Atmos., 113, D09104, doi:10.1029/2007JD009263, 2008.

Santer, B. D., Mears, C., Doutriaux, C., Caldwell, P., Gleckler, P. J., Wigley, T. M. L., Solomon, S., Gillett, N. P., Ivanova1, D., Karl, T. R., Lanzante, J. R., Meehl, G. A., Stott, P. A., Taylor, K. E., Thorne, P. W., Wehner, M. F., and Wentz, F. J.: Separating signal and noise in atmospheric temperature changes: The importance of timescale, J. Geophys. Res., 116, D22105, doi:10.1029/2011JD016263, 2011.

Scanlon, B. R., Reedy, R. C., and Gates, J. B.: Effects of irrigated agroecosystems: 1. Quantity of soil water and groundwater in the southern High Plains, Texas, Water Resour. Res., 46, W09537, doi:10.1029/2009WR008427, 2010.

Sharma, K. P., Moore, B., and Vorosmarty, C. J.: Anthropogenic, climatic, and hydrologic trends in the Kosi Basin, Himalaya, Clim. Change, 47, 141–165, 2000.

Snyder, R. L., Orang, M., Matyac, S., and Grismer, M. E.: Simplified estimation of reference evapotranspiration from pan evaporation data in California, J. Irrig. Drain. Eng.-Asce, 131, 249–253, 2005.

Su, Z.: The Surface Energy Balance System (SEBS) for estimation of turbulent heat fluxes, Hydrol. Earth Syst. Sci., 6, 85–100, doi:10.5194/hess-6-85-2002, 2002.

Su, Z., Schmugge, T., Kustas, W. P., and Massman, W. J.: An evaluation of two models for estimation of the roughness height for heat transfer between the land surface and the atmosphere, J. Appl. Meteorol., 40, 1933–1951, 2001.

Taylor, R. G., Scanlon, B., Doll, P., Rodell, M., van Beek, R., Wada, Y., Longuevergne, L., Leblanc, M., Famiglietti, J. S., Edmunds, M., Konikow, L., Green, T. R., Chen, J., Taniguchi, M., Bierkens, M. F. P., MacDonald, A., Fan, Y., Maxwell, R. M., Yechieli, Y., Gurdak, J. J., Allen, D. M., Shamsudduha, M., Hiscock, K., Yeh, P. J. F., Holman, I., and Treidel, H.: Ground water and climate change, Nat. Clim. Change 3, 322–329, 2013.

Teuling, A. J., Hirschi, M., Ohmura, A., Wild, M., Reichstein, M., Ciais, P., Buchmann, N., Ammann, C., Montagnani, L., Richardson, A. D., Wohlfahrt, G., and Seneviratne, S. I.: A regional perspective on trends in continental evaporation, Geophys. Res. Lett., 36, L02404, doi:10.1029/2008GL036584, 2009.

Tiwari, V. M., Wahr, J., and Swenson, S.: Dwindling groundwater resources in northern India, from satellite gravity observations, Geophys. Res. Lett., 36, L18401, doi:10.1029/2009GL039401, 2009.

Verhoef, W., Menenti, M., and Azzali, S.: A colour composite of NOAA-AVHRR-NDVI based on time series analysis (1981–1992), Int. J. Remote Sens., 17, 231–235, 1996.

Vinukollu, R. K., Wood, E. F., Ferguson, C. R., and Fisher, J. B.: Global estimates of evapotranspiration for climate studies using multi-sensor remote sensing data: Evaluation of three process-based approaches, Remote Sens. Environ., 115, 801–823, 2011.

Wada, Y., van Beek, L. P. H., and Bierkens, M. F. P.: Nonsustainable groundwater sustaining irrigation: A global assessment, Water Resour. Res., 48, W00L06, doi:10.1029/2011WR010562, 2012.

Wang, Q., Adiku, S., Tenhunen, J., and Granier, A.: On the relationship of NDVI with leaf area index in a deciduous forest site, Remote Sens. Environ., 94, 244–255, 2005.

Yang, D. W., Sun, F. B., Liu, Z. Y., Cong, Z. T., Ni, G. H., and Lei, Z. D.: Analyzing spatial and temporal variability of annual water-energy balance in nonhumid regions of China using the Budyko hypothesis, Water Resour. Res., 43, W04426, doi:10.1029/2006WR005224, 2007.

Zhang, K., Kimball, J. S., Mu, Q. Z., Jones, L. A., Goetz, S. J., and Running, S. W.: Satellite based analysis of northern ET trends and associated changes in the regional water balance from 1983 to 2005, J. Hydrol., 379, 92–110, 2009.

Zhang, L., Dawes, W. R., and Walker, G. R.: Response of mean annual evapotranspiration to vegetation changes at catchment scale, Water Resour. Res., 37, 701–708, 2001.

Zhang, Q., Jiang, T., Gemmer, M., and Becker, S.: Precipitation, temperature and runoff analysis from 1950 to 2002 in the Yangtze basin, China, Hydrolog. Sci. J., 50, 65–80, 2005.

Zhang, X. B., Zwiers, F. W., Hegerl, G. C., Lambert, F. H., Gillett, N. P., Solomon, S., Stott, P. A., and Nozawa, T. Detection of human influence on twentieth-century precipitation trends, Nature, 448, 461–465, 2007.

Zhang, Y. Q., Liu, C. M., Tang, Y. H., and Yang, Y. H.: Trends in pan evaporation and reference and actual evapotranspiration across the Tibetan Plateau, J. Geophys. Res.-Atmos., 112, D12110, doi:10.1029/2006JD008161, 2007.

Zhang, Y. Q., Leuning, R., Chiew, F. H. S., Wang, E. L., Zhang, L., Liu, C. M., Sun, F. B., Peel, M. C., Shen, Y. J., and Jung, M.: Decadal Trends in Evaporation from Global Energy and Water Balances, J. Hydrometeorol., 13, 379–391, 2012.